Random walks on B distributed resting-state functional connectivity to identify Alzheimer's disease and Mild Cognitive Impairment

Mohammadmahdi Rahimiasl, Nasrollah Moghadam Charkari *, Foad Ghaderi,
For the Alzheimer's Disease Neuroimaging Initiative [1]

Department of Electrical and Computer Engineering, Tarbiat Modares University, Tehran, Tehran, Iran

ARTICLE INFO

HIGHLIGHTS

- An accurate way of classifying Alzheimer's Disease and Mild Cognitive Impairment is presented in this article.
- The B distributed mapping function is proposed for constructing brain networks.
- Node2vec algorithm proved to be an accurate algorithm for extracting features from brain networks.

ABSTRACT

Objective: Resting-state functional connectivity reveals a promising way for the early detection of dementia. This study proposes a novel method to accurately classify Healthy Controls, Early Mild Cognitive Impairment, Late Mild Cognitive Impairment, and Alzheimer's Disease individuals.
Methods: A novel mapping function based on the B distribution has been developed to map correlation matrices to robust functional connectivity. The node2vec algorithm is applied to the functional connectivity to produce node embeddings. The concatenation of these embedding has been used to derive the patients' feature vectors for further feeding into the Support Vector Machine and Logistic Regression classifiers.
Results: The experimental results indicate promising results in the complex four-class classification problem with an accuracy rate of 97.73% and a quadratic kappa score of 96.86% for the Support Vector Machine. These values are 97.32% and 96.74% for Logistic Regression.
Conclusion: This study presents an accurate automated method for dementia classification. Default Mode Network and Dorsal Attention Network have been found to demonstrate a significant role in the classification method.
Significance: A new mapping function is proposed in this study, the mapping function improves accuracy by 10–11% in the Alzheimer's Disease Neuroimaging Initiative (ADNI) database.

1. Introduction

Alzheimer's disease (AD) is a continuum neurodegenerative disease that causes unchanging cognitive decline and neurodegenerative dysfunction. The presence of β-amyloid plaques and neurofibrillary tau deposits identifies AD (Dubois et al., 2016; Jack et al., 2018). It has been found that getting older promotes disease progression (Brookmeyer et al., 2007). Mild Cognitive Impairment (MCI) is an intermediary stage between healthy aging and dementia. Also, MCI patients turn into AD ones at the rate of 10–15% every year; it is a tremendous rate compared to the 1–2% risk

* Corresponding author.
E-mail addresses: m.rahimiasl@modares.ac.ir (M. Rahimiasl), moghadam@modares.ac.ir (N. Moghadam Charkari), fghaderi@modares.ac.ir (F. Ghaderi).

of healthy aging transition to AD (Misra et al., 2009). There is no specific treatment for Alzheimer's disease. However, early detection of the disease helps plan for care and living arrangements, research new diagnostic methods, examine new medications, and experiment with strategies to prevent disease development (Paquerault, 2012).

Consequently, the diagnosis of the progression of AD and other stages of dementia are prominent. Researchers put much work into developing algorithms and methods to detect different stages of AD and dementia to tackle this requirement. This work is done using data from various neuroimaging methods, including Positron Emission Tomography (PET) (Duara et al., 2013), ElectroEncephaloGram (EEG) (Lehmann et al., 2007), Magnetoencephalography (MEG) (Engels et al., 2016), and functional Magnetic Resonance Imaging (fMRI) (Sheng et al., 2020).

Resting-state functional Magnetic Resonance Imaging (rs-fMRI) is a non-invasive neuroimaging technique with a high spatial and moderate temporal resolution. Accordingly, the blood-oxygenation level-dependent (BOLD) signal is used to measure spontaneous low-frequency fluctuations. Some studies have been leveraged rs-fMRI's BOLD signals to construct a functional connectivity network (FCN) of the brain. Then, the interactions between different brain regions are undertaken by FCN features to diagnose AD and MCI (Wang et al., 2018). Studies have employed various types of functional connectivity networks. However, most of the methods have used stationary FCNs. (Bi et al., 2018a, 2018b; Khazaee et al., 2015). However, some studies have also used dynamic FCNs (Jie et al., 2018). (Chen et al., 2016) proposed a High Order Resting-State Functional Connectivity method for detecting Early Mild Cognitive Impairment (EMCI) patients from healthy controls (HC). There have been several types of features extracted from FCNs for further use in classifiers. Some of these features include edge weights (Bi et al., 2018a; Zhang et al., 2015) and the graph metrics like Node strengths, Node degrees(Sheng et al., 2019), clustering coefficients (de Vos et al., 2018), betweenness centrality (Sheng et al., 2019), eigenvector centrality (Son et al., 2017), and Pagerank (Sheng et al., 2019). A few studies have leveraged graph embedding methods such as graph kernel (Sharaev et al., 2019). (Tang et al., 2019) introduced an algorithm based on random walks similar to node2vec to classify stages of MCI on brain networks derived from MRI images.

There exist several atlases for parcellated analysis of the brain. Automatic Anatomical Labeling (AAL) (Tzourio-Mazoyer et al., 2002), 264 putative functional areas (Power et al., 2011), Harvard-Oxford Cortical/Subcortical Atlas (Makris et al., 2006), and Yeo 2011 functional parcellations (Yeo et al., 2011Buckner et al., 2011) are some of the available atlases. Most studies use the AAL atlas to parcellate the brain into 90 or 116 regions (Bi et al., 2018b, 2018a; Jie et al., 2018; Khazaee et al., 2015). Parcellated analysis improves the signal-to-noise ratio (SNR) by averaging each region's time series (Glasser et al., 2016). Thus, more accurate parcellation leads to better results. (Khazaee et al., 2016) showed how three HC, MCI, and AD groups could be appropriately classified with an accuracy rate of 88.4% using 264 putative functional areas atlas.

Many studies have used brain parcellation based on one neurobiological property such as architecture, function, connectivity, or topography. HCP-MMP atlas (Glasser et al., 2016) combines multiple Neurobiological properties and delineates 180 areas per hemisphere from a group of 210 healthy young adults. The studies suggest that HCP-MMP is the most detailed cortical parcellation available in vivo[2]. (Sheng et al., 2019) applied this parcellation to

get competitive results in AD, EMCI, and Late Mild Cognitive Impairment (LMCI) classification. The same parcellation was also used by (Sheng et al., 2020) to classify HC, AD, and MCI in another study. In some studies, the binary functional brain network was generated from the correlation matrix using an adaptive or static threshold. Other researchers have used the bare correlation matrix or the normalized correlation matrix (using Fisher r-to-z transformation) as their weighted FCNs.

This study proposes a method for automatically and efficiently classifying AD, EMCI, and LMCI patients using some new features that have not previously been explored. The details of the proposed method are shown in Fig. 1.

2. Methods

2.1. Subjects

"Data used in the preparation of this article were obtained from the Alzheimer's Disease Neuroimaging Initiative (ADNI) database (adni.loni.usc.edu). The ADNI was launched in 2003 as a public–private partnership, led by Principal Investigator Michael W. Weiner, MD. The primary goal of ADNI has been to test whether serial magnetic resonance imaging (MRI), positron emission tomography (PET), other biological markers, and clinical and neuropsychological assessment can be combined to measure the progression of mild cognitive impairment (MCI) and early Alzheimer's disease (AD)."

Twenty-six AD, Thirty EMCI, Thirty-three LMCI patients, and Thirty-six healthy controls with available resting-state fMRI data have been adopted. (Xue et al., 2019; Zhang et al., 2019) provides more information about ADNI's data collection protocol and diagnostic criteria of AD, MCI, and HC. Subjects with more than 2 mm head translation, 2 degrees head rotation, Maximum framewise displacements (FD) of more than 5 mm, mean FD of more than 0.5 mm, and more than 90 out of 130 timesteps removed in the motion scrubbing process have been discarded. Table 1 presents additional information on the remaining subjects.

2.2. Synthetic dataset

The proposed method is further examined by creating a synthetic dataset with a conventional method. A normal distribution is fitted to each individual's weight strength from the preprocessed brain network from the ADNI database. The fitted distributions provide mean and standard deviation parameters. Then, a synthetic brain network is drawn from these parameters. Fig. 2 presents a fitted distribution for a healthy control individual.

2.3. Preprocessing

These data were preprocessed by fMRIPrep 1.5.6 (Esteban et al., 2019, 2018), an fMRI preprocessing pipeline software developed using Nipype 1.4.0 (Esteban et al., 2020; Gorgolewski et al., 2011).

2.3.1. Anatomical data preprocessing

N4BiasFieldCorrection (Tustison et al., 2010), part of ANTs 2.2.0 registration suite (Avants et al., 2008), was used to correct intensity non-uniformity (INU) of the T1-weighted images. During the workflow, the corrected image is used as a T1w-reference. T1w-reference was skull stripped using antsBrainExtraction.sh, and OASIS30ANTs were used as the target template. The segmentation of the brain into different tissue types (white matter (WM), cerebrospinal fluid (CSF), and gray matter (GM)) was done using the fast function from FSL 5.0.9 (Zhang et al., 2001). Recon-all program from FreeSurfer 6.0.1 (Dale et al., 1999) was used to reconstruct

---

[2] https://www.lead-dbs.org/helpsupport/knowledge-base/atlasesresources/cortical-atlas-parcellations-mni-space/
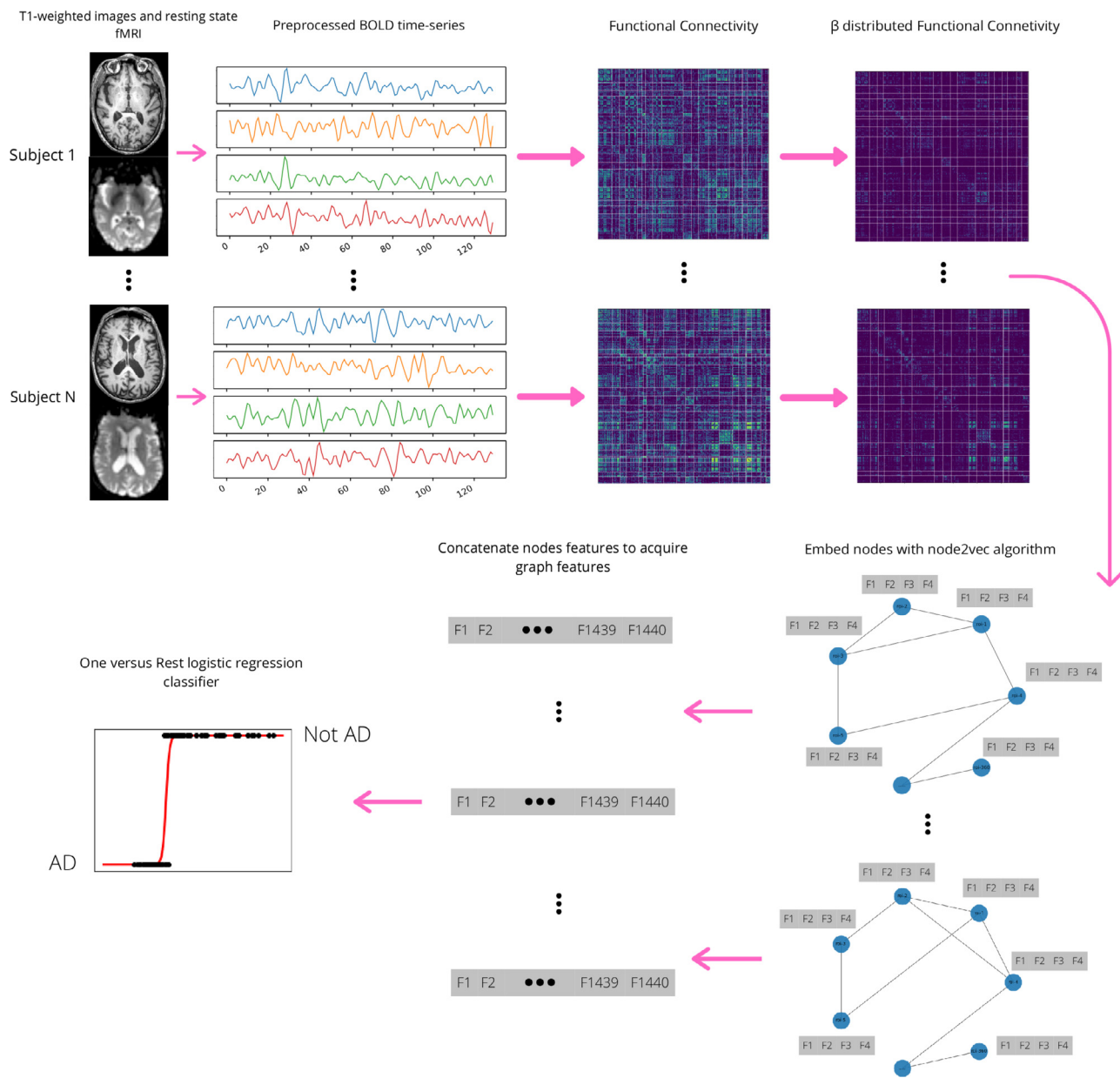
Fig. 1. The proposed framework in this study. Note that T1 weighted images have been used in the preprocessing steps. AD: Alzheimer's Disease.

Table 1
Basic information of selected participants. HC: Healthy Control, EMCI: early Mild Cognitive Impairment, LMCI: late Mild Cognitive Impairment, AD: Alzheimer's Disease.

	HC	EMCI	LMCI	AD
No of subjects	36	30	33	26
Age(Mean ± SD)	75.78 ± 5.83	71.67 ± 7.50	71.76 ± 7.28	73.96 ± 7.63
Gender(Female/Male)	22/14	16/14	15/18	14/12

brain surfaces. A custom method to provide ANTs-derived and FreeSurfer-derived segmentation of Mindboggle's cortical gray matter (Klein et al., 2017) was used to fine-tune previously evaluated brain mask. The ICBM 152 Nonlinear Asymmetrical template version 2009c (MNI152NLin2009cAsym) (Fonov et al., 2009) was chosen for volume-based spatial normalization. ANTs 2.3.3′s antsRegistration was used for nonlinear spatial normalization.

2.3.2. Functional data preprocessing

As a first step, a reference volume and skull-stripped version were created using a method implemented in fMRIPrep for each of the 1 BOLD runs for each subject. A deformation field is calculated to correct distortions caused by Echo-planar Imaging (EPI) based on fMRIPrep's fieldmap-less approach. An inverted intensity's T1w-reference is co-registered with the BOLD reference to
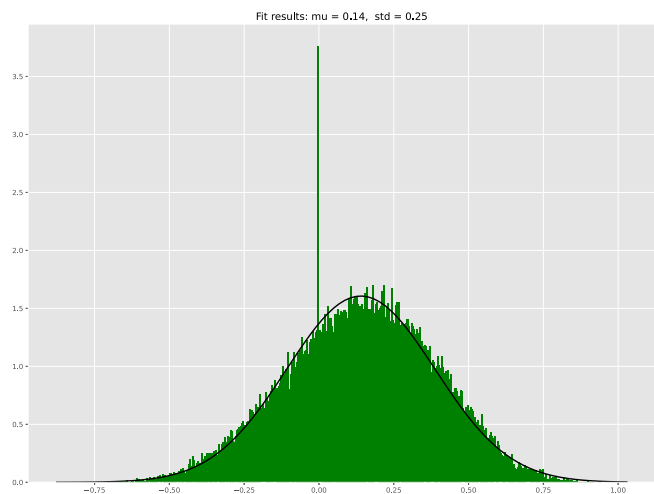
Fig. 2. Normal distribution fitted to the edge weights of one of the healthy control brain's network.

determine the deformation field (Huntenburg et al., 2014; Wang et al., 2017). antsRegistration is used for registration. Only nonzero values over the phase encoding direction are allowed during the process to regulate the deformation, and a field map template is used to modulate it (Treiber et al., 2016). Correction of the EPI reference was calculated using the estimated susceptibility distortion to co-register with anatomical reference accurately. Using FreeSurfer's bbregister program, a boundary-based registration (Greve and Fischl, 2009) was applied to co-register BOLD with T1w reference. This co-registration had nine degrees of freedom to eliminate the remaining distortions in the BOLD reference. Prior to spatiotemporal filtering using the mcflirt tool from FSL 5.0.9 (Jenkinson et al., 2002), the BOLD reference's head motion is estimated through transformation matrices and six rotation and translation parameters. The BOLD time series was resampled to fsaverage5 surface to correct distortions due to head movement and susceptibility. BOLD time series were resampled using a single composite transform. In this paper, BOLD time series that are resampled is called preprocessed BOLD in original space or preprocessed BOLD for conciseness. Then preprocessed BOLD time-series were resampled into the ['MNI152NLin2009cAsym'] space. The first step was to generate a reference volume and its skull-stripped version using fMRIPrep's custom methodology.

The following signals were calculated after preprocessing the BOLD: three region-wise global signals, DVARS, and FD. Nipype implementations are used for FD and DVARS computations (Power et al., 2014). Global signals are generated inside the WM, CSF, and whole-brain masks. For component-based noise reduction, several physiological variables were extracted (Behzadi et al., 2007)(CompCor). Discrete cosine high-pass filter with a cut-off of 128 seconds is applied to the preprocessed BOLD time-series separated into temporal and anatomical ComCor variants (tCompCor and aCompCor, respectively) for estimating their principal components. The tCompCor is extracted from the 5% highest variable voxels within masks that cover the subcortical regions. The brain mask is massively eroded to obtain this subcortical mask, ensuring that it is exempt from GM regions in the cortex. Components of aCompCor are computed by applying the above-referenced mask's intersection with the combination of the WM and CSF masks based on the anatomical space. Within the WM and CSF masks, components are also calculated separately. The k leading components from each CompCor decomposition are kept. The time series of these kept components are enough to account for half of the variance over nuisance masks. As part of the correc-

tion step, the head-motion measurements were also placed into the corresponding confounding file. The time series of confounds was extended by including quadratic and temporal terms for head motions and global signals (Satterthwaite et al., 2013). Motion outliers were defined as frames that exceeded the FD threshold of 0.5 or the DVARS threshold of 1.5. All resamplings can be performed in a single interpolation step by composing head-motion, susceptibility distortion correction, and co-registrations to anatomical and output spaces transformations. To reduce the smoothing effects of other kernels, gridded (volumetric) resamplings were carried out using antApplyTransforms with Lanczos interpolation configuration (Lanczos, 1964). FreeSurfer's mri_vol2surf was used for non-gridded surface resamplings.

fMRIPrep uses Nilearn 0.6.1 internally (Abraham et al., 2014), mainly as part of the functional processing procedure. The fMRI-Prep documentation offers more details on the pipeline.

Ten thousand and two-hundred and forty-two time-series vertices per hemisphere (20484 total) on fsaverage5 space have been obtained from the output of fMRIPrep. Then, the first ten volumes are discarded. Linear detrending, temporal bandpass filtering (0.01 Hz – 0.08 Hz), and confounds regression has been performed using the Nilearn python library (signal clean method) (Abraham et al., 2014). Confound regression has been conducted orthogonally to temporal filters with the following parameters: head motion parameters (Satterthwaite et al., 2013), global signal, cerebrospinal fluid, framewise displacement, white matter, aCompCor (Muschelli et al., 2014), std dvars, and cosine nuisances (Friston et al., 1994; Lindquist et al., 2018). Motion scrubbing is performed with an FD threshold value of 0.5 and a timepoint window removal length of 10 (Power et al., 2014). In our experiments, we used some of the source code and data publicly available at the Brain Networks course repository maintained by the department of psychology at Stanford University[3].

2.4. Functional connectivity networks

Graphs or networks play a significant role in demonstrating the human brain's functional and structural connectivity by modeling the brain regions as nodes and the connections between them as edges. There are two types of edges in graph theory: weighted and unweighted (binary) edges. In graphs with binary edges, edges can be present or absent. They do not provide further information about the strength of the connection between two brain regions. On the other hand, weighted graphs provide the strength of connections between brain regions. In rs-fMRI studies (Chen et al., 2016; Wang et al., 2018), functional connectivity is mainly formed by establishing a correlation between the average time series within brain regions. These correlations might be further used to construct a correlation matrix. Correlation matrices need to be processed so that they can be utilized as functional connectivity networks. There are two standard methods available to handle negative values in correlation matrices. These values can be set to zero or be replaced by their absolute values. Also, It is a common choice to set self-correlations to zero (Rubinov and Sporns, 2010). In this study, the first approach has been employed to handle negative values.

Let us assume half the weights are positive. Consider r as the number of nodes in the graph. The result is a network whose number of edges is $r(r − 1)/4$ when negative values are converted to zeros and $r(r − 1)/2$ when replaced with their absolute values. This approach leads to a dense network. For the HCP-MMP atlas, the number of edges for the scenarios mentioned earlier is 32,310 and 64,620 for only 360 nodes. Some studies employed a thresh-

---

[3] https://github.com/BrainNetworksCourse/brain-networks-course/

olding approach to deal with this degree of complexity (Bi et al., 2018b). In the thresholding approach, a correlation matrix is constructed by setting values below the threshold to zeros while the remaining values are set to ones or remain the same. A graph with a more significant threshold value will be more sparse. Several heuristics have been introduced to help evaluate the threshold value more accurately. For instance, (Son et al., 2017) proposed a method to find the threshold value so that the graph remains strongly connected. In this study, the average time series for each brain region within 360 discrete regions in the HCP-MMP atlas (Glasser et al., 2016) is calculated. Then, Pearson's correlation has been evaluated between each pair of the averaged time-series to determine the correlation matrices.

2.5. B distributed mapping function

In this paper, the following function is proposed to map the processed correlation matrices to functional connectivity networks:

Equation (1)

$$f(x) = x \times B(x; \alpha, \beta) \qquad (1)$$

where the B is a continuous probability distribution function, it has the following properties that make it beneficial for mapping correlation values to the brain's functional connectivity's connection strength: It is bounded on the interval [0,1], two positive parameters, α, and β form the shape of the distribution, for $\alpha \geq 1$ and $\beta \leq 1$, the probability density function (PDF) of the B distribution is monotonically increasing. It is a flexible distribution that makes it possible to achieve squeezing and expanding properties. For $\alpha > 1$ and $\beta \leq 1$, small values are converted into near-zero numbers, while larger values are transformed into more significant numbers.

This mapping function's squeezing and expanding properties scales the input value in a nonlinear manner, reinforcing the vital information of the FCN while vanishing the negligible correlations between the nodes. Consider two correlation values of 0.5 and 0.9; the first value is typical and happens between many time series. In contrast, the second value is rare, and time-series correlated with the amount of 0.9 are strongly correlated. The second link is only 80% stronger than the first link without using the proposed mapping function. However, by applying this mapping function, with parameters $\alpha = 2$ and $\beta = 1$, the second link value changes to 1.62 and becomes 224% stronger. In Fig. 3, this function with different α values, while β is fixed at one, has been compared. In Figs. 4 and 5, the functional connectivity network of a healthy control is depicted. These images compare functional connectivity with and without employing the proposed mapping function.

For different α parameter values, the connection strengths scale varies in the connectivity networks derived from this mapping function. The maximum value can be equal to the amount of α for input equal to 1. However, Due to the removal of the nodes' self-correlations, the values are smaller in practice. This value might differ for each participant.

2.6. Node2Vec

Recent developments in deep learning, especially in natural language processing (Mikolov et al., 2013), have led several studies to extend language models to graph representation learning(Perozzi
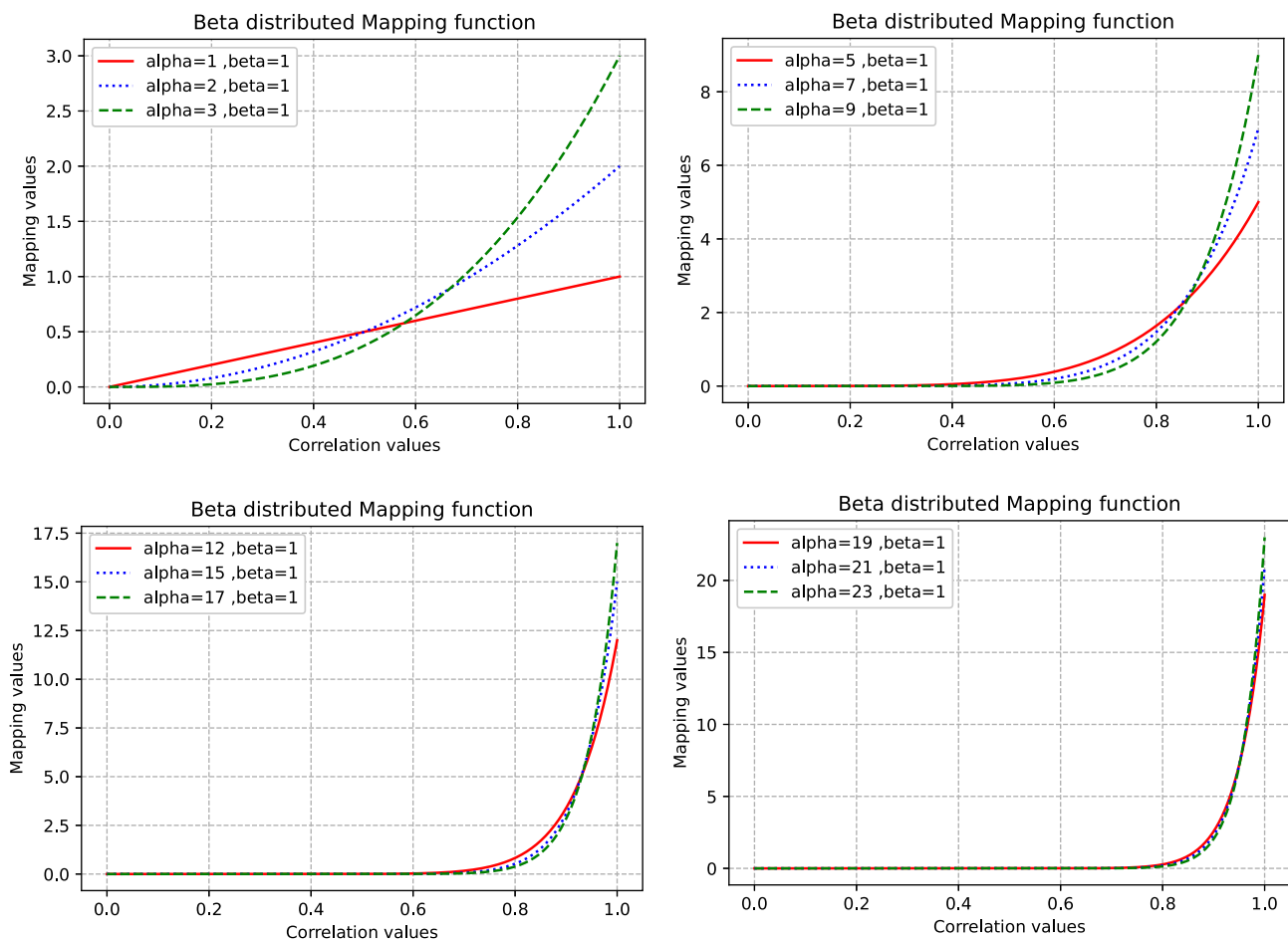

Fig. 3. B distributed mapping function for different values of α. As α increases, the expanding and squeezing properties become stronger.
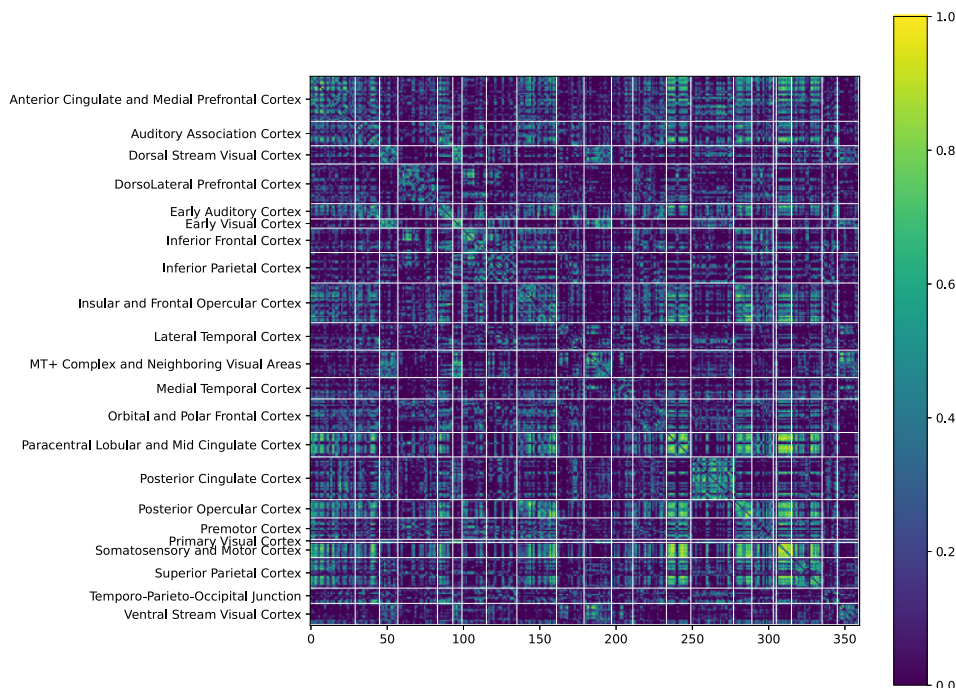
Fig. 4. Functional connectivity network without using the proposed mapping function.

et al., 2014; Tang et al., 2015). These models mainly consider a graph as a document and sequences of random walks as sequences of words in a document. The method proposed in (Grover and Leskovec, 2016) is a successful graph representation learning algorithm that uses a second-order random walk approach to generate walk sequences. Let G = (V, E) be the brain network. The objective of node2vec is to learn a mapping function $f: V \rightarrow R^d$, where d is a parameter defined as the feature dimension size, and V is denoted

as the node-set of the graph. The function is derived by optimizing the following objective function:

Equation (2)

$$max_f \sum_{u \in V} \log Pr(N_S(u)|f(u)) \tag{2}$$

for every node u in node-set V, $N_s(u)$ is defined as the network neighborhood of node u. In summary, this equation optimizes a mapping function from a graph to an embedding space in which
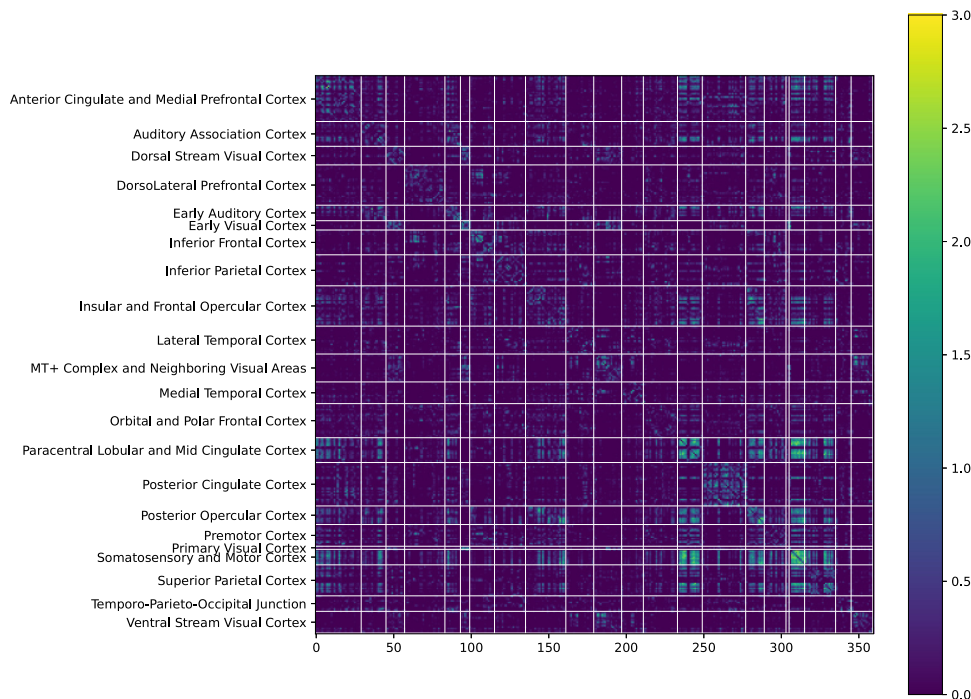

Fig. 5. Functional connectivity network using the proposed mapping function.

similar nodes in the original graph are close to each other in the embedding space. The closeness of two nodes in the embedding space can be defined as a dot product between two embeddings.

Node2vec employs a second-order random walk algorithm to calculate the nodes' network neighborhood. This procedure receives two parameters; parameter p (return parameter) controls the possibility of instantly revisiting a node in the walk. Furthermore, parameter q is defined as the in-out parameter that enables the search possibility to distinguish between "inward" and "outward" nodes. The transition probability of traversing from node v to node x when the random walker has just crossed the edge (t, v) derived from this procedure is equal to $\pi_{vx} = \alpha_{pq}(t, x)\hat{A} \cdot \omega_{vx}$, where ω_{vx} indicates the edge weight (for unweighted graphs $\omega_{vx} = 1$), and:

Equation (3)

$$\alpha_{pq}(t, x) = \begin{cases} \frac{1}{p} \, if \, d_{tx} = 0 \\ 1 \, if \, d_{tx} = 1 \\ \frac{1}{p} \, if \, d_{tx} = 2 \end{cases} \tag{3}$$

d_{tx} indicates the shortest path between nodes t and x. Further information about node2vec is provided in the original paper (Grover and Leskovec, 2016). This study utilizes small node embedding (size = 4) calculated from short random walks (walk length = 10). Graph embeddings are derived from concatenating node embeddings. The reason for employing this embedding size is to ensure that embedding contains sufficient information about each node leading to a good representation of the whole brain network, but not too much redundant information causing the curse of dimensionality. Furthermore, since graphs are embedded using the concatenation of each node's embeddings, short random walks are applied so that each node only contains information about its adjacent neighboring.

2.7. Classification and evaluation criteria

This study used L2 regularized logistic regression (Zhu et al., 1997) and linear support vector machine classifiers (Chang and Lin, 2011; Fan et al., 2008). Linear classifiers such as logistic regres-

Table 2
Comparing different approaches for the classification of Alzheimer's disease and mild cognitive impairments. As shown, most of these works have used two-class classification, while few have investigated three classes. HC: Healthy Control, EMCI: early Mild Cognitive Impairment, LMCI: late Mild Cognitive Impairment, AD: Alzheimer's Disease, SVM: Support Vector Machine, LR: Logistic Regression, LASSO: least absolute shrinkage and selection operator, LDA: linear discriminant analysis. The first seven methods classify two stages. The following three methods classify three stages of HC, MCI, and AD. Our approach classifies four stages of HC, EMCI, LMCI, and AD.

| Study	Participants	Short description	Performance
(Khazaee et al., 2015)	HC = 20 AD = 20	Various features are considered, such as average path length, average clustering coefficient, and others, to feed into the SVM classifier.	ACC = 100%
(Jie et al., 2014)	HC = 25 MCI = 12	This study employs Weisfeiler Lehman Graph kernels in the multilevel network to generate features, LASSO for feature selection, and SVM as the classifier.	ACC = 91.9%
(Bi et al., 2018a)	HC = 25 AD = 35	Functional connectivity edge weights are used as features in this study, while ensembles of the SVM are used as the classifier. A random selection of features and subjects was applied to each SVM classifier.	ACC = 94.4%
(Jie et al., 2018)	HC = 50 EMCI = 56 LMCI = 43	BOLD time-series were segmented into non-overlapping windows, and Pearson correlations were used to construct temporal nets. Spatial and temporal variability were utilized as features, gLASSO was used for feature selection, and SVM was used as the classifier.	ACC = 78.8% LMCI vs. EMCI ACC = 78.3% EMCI vs. HC
(Sheng et al., 2019)	HC = 24 EMCI = 24 LMCI = 24 AD = 24	The classifier used in this study is the SVM, and its features include node strength, degree, clustering coefficient, local efficiency, betweenness, and other measures derived from functional connectivity in the HCP-MMP atlas.	ACC = 93.8% EMCI vs. HC ACC = 95.8% LMCI vs. HC ACC = 95.8% AD vs. HC
(Tang et al., 2019)	EMCI = 72 LMCI = 39	This study proposes a random walk embedding method in structural connectivity to classify participants using an SVM classifier.	ACC = 72.4%
(Zhang et al., 2019)	EMCI = 33 LMCI = 29	In this study, Functional connectivity is modeled using different frequency bands, global and local efficiency, clustering coefficient, and characteristic path length were utilized as features. Minimal redundancy, maximum relevance, sparse linear regression feature selection, and fisher score methods were employed for feature selection.	ACC = 83.3%
(Son et al., 2017)	HC = 35 MCI = 40 AD = 30	A random forest classifier is used to classify subjects in this study using eigenvector centralities as the features.	ACC = 53.3%
(Wang et al., 2018)	HC = 12 MCI = 11 AD = 10	In this study, clustering coefficients serve as features, regularized LDA to reduce noise, and ADA boost as the classifier.	ACC = 75.8%
(Sheng et al., 2020)	HC = 24 MCI = 24 AD = 24	The features in this study include node strength, betweenness centrality, clustering coefficient, and six other measures of the network from the HCP-MMP brain atlas. Logistic regression recursive feature elimination algorithm is employed for feature selection, and linear SVM is used as the classifier.	ACC = 88%
Our method	HC = 36 EMCI = 30 LMCI = 33 AD = 25	Results of this study for the ADNI database without using the proposed mapping function.	ACC = 87.2% SVM classifier ACC = 86.96% LR classifier
Our method	HC = 36 EMCI = 30 LMCI = 33 AD = 25	Results of this study for the ADNI database using the proposed mapping function.	ACC = 97.736% SVM classifier ACC = 97.328% LR classifier
Our method	HC = 36 EMCI = 30 LMCI = 33 AD = 25	Results of this study for the synthetic database without using the proposed mapping function.	ACC = 96.216% SVM classifier ACC = 96.624% LR classifier
Our method	HC = 36 EMCI = 30 LMCI = 33 AD = 25	Results of this study for the synthetic database using the proposed mapping function.	ACC = 98.128% SVM classifier ACC = 98.552% LR classifier
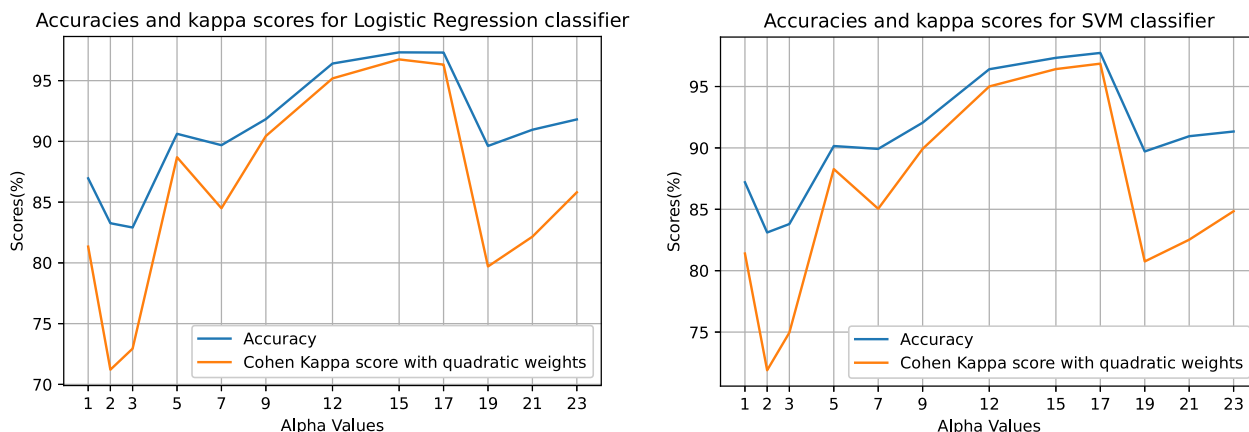
Fig. 6. Accuracy and Kappa score for different values of α. SVM: Support Vector Machine.

sion and linear support vector machines are resilient to overfitting. The pipeline is evaluated through fivefold cross-validation. The cross-validation procedure is repeated 100 times to avoid noisy model performance.

The random walk procedure can be controlled by the Node2vec algorithm with two independent variables called p and q, which are fixed at one in this study. This procedure is applied for the following α values: 1,2,3,5,7,9,12,15,17,19,21,23, and the β value remains a constant of one for all cases. Note that, when α = β = 1 , this mapping function returns its input.

This study reports the accuracy and the quadratic weighted Cohen's kappa score (Cohen, 1968) in the final results. Accuracy is a simple criterion that measures the proportion of the correctly classified samples to the number of all samples. While accuracy is vital for classifiers, it leaves out some essential information. Imagine two different classification schemes, one of which wrongly classifies an Alzheimer's patient as Healthy Control, and the other misclassifies the patient as Late Mild Cognitive Impairment. The accuracy of both classifiers is the same. However, the second classifier outperforms the first one because Late Mild Cognitive Impairment is more like Alzheimer's disease than Healthy Control.

Multiclass classification in medical tasks is plagued with this problem.

Nevertheless, the problem can be solved using the Kappa score. Kappa score is a statistic that measures the agreement between the classifier and the expert diagnosis. The kappa score of one indicates complete agreement, zero indicates random agreement, and negative values indicate worse than a random agreement between raters. The quadratic weighted kappa score employs a quadratic weight for the distance of misclassification. Considering the two classifiers mentioned above, the second gets a penalty of one, while the first gets nine ($= 3^2$).

2.8. Nodes importance calculation

The normalized coefficient magnitude of the logistic regression classifier for each feature is initially found to further calculate each node's importance. This value indicates the importance of an element. Each node is represented using four values. To calculate the significance of the nodes, features corresponding to each node are summed to obtain node importance. The cumulative values are normalized to add up to 1 to express these values by percentages.

Table 3

Importance of features based on the brain cortexes and the yeodesc7 network assignments. HC: Healthy Control, EMCI: early Mild Cognitive Impairment, LMCI: late Mild Cognitive Impairment, AD: Alzheimer's Disease. The numbers indicate the cortexes and regions by percentage.

Cortex name/Importance (%)	CN	EMCI	LMCI	AD	Region/Importance(%)	CN	EMCI	LMCI	AD
posterior cingulate cortex	8.19	11.20	7.73	7.97	default	21.43	31.19	22.30	23.89
anterior cingulate and medial prefrontal cortex	8.93	9.56	7.26	8.31	visual	12.27	13.64	18.58	17.63
dorsolateral prefrontal cortex	8.41	8.73	7.74	8.46	Somato motor	14.66	13.78	14.90	13.60
mt + complex and neighboring visual areas	3.70	4.86	6.64	5.43	dorsal attention	15.59	9.27	15.73	13.19
inferior parietal cortex	6.80	5.88	5.90	5.91	frontoparietal	13.55	13.20	11.66	13.62
superior parietal cortex	7.97	3.85	7.97	5.63	ventral attention	15.40	10.83	10.72	11.31
insular and frontal opercular cortex	7.38	6.51	5.74	6.34	limbic	7.07	8.05	6.08	6.72
medial temporal cortex	4.21	3.42	2.69	3.23					
inferior frontal cortex	3.73	4.39	3.55	5.00					
auditory association cortex	3.05	4.53	4.14	3.63					
lateral temporal cortex	4.34	5.31	4.38	4.57					
orbital and polar frontal cortex	5.12	7.05	5.06	6.22					
ventral stream visual cortex	2.97	2.90	4.09	4.45					
paracentral lobular and mid cingulate cortex	5.33	3.84	4.08	3.89					
dorsal stream visual cortex	2.88	2.88	4.53	3.97					
early auditory cortex	2.30	2.64	3.02	2.30					
posterior opercular cortex	3.57	3.11	3.12	2.83					
somatosensory and motor cortex	2.98	2.35	2.74	2.55					
premotor cortex	4.59	2.74	3.63	4.00					
early visual cortex	0.88	1.51	2.55	2.30					
temporo-parieto-occipital junction	2.14	2.24	2.74	2.19					
primary visual cortex	0.42	0.39	0.60	0.60					

Furthermore, aggregating each node's importance in the cortexes' importance has been calculated based on the information from (Glasser et al., 2016).

Consequently, MMP regions would be mapped to the yeo network assignments (Buckner et al., 2011) for better comparison with the other studies. Since the one vs. rest method is used in this study, the importance of each class could be found.

3. Results

The proposed method presents a trustworthy representation of the brain connectivity network, leading to promising results in the classification of Healthy Controls and individuals with EMCI, LMCI, and AD. Support vector machine and Logistic regression classifiers both provide similar results using the proposed mapping function. It provides ten percent improvement in accuracy and fifteen percent improvement in quadratic kappa scores for the ADNI database. For the synthetic database, these numbers are about two and one percent, respectively. One thing that stands out in this study is that all dementia stages can be classified using a single pipeline. The majority of the studies employ a binary classification. A summary of different studies on dementia classification is presented in Table 2. As is evident from Table 2, many of these works examined binary classification. Moreover, fewer studies focused on the three-class dementia problem. Fig. 6 provides a comparison of accuracy and kappa scores with different α values.

In the classification of dementia, important cortices were the posterior cingulate cortex, the dorsolateral prefrontal cortex, the anterior cingulate, and the medial prefrontal cortex. Cortexes mentioned above are part of DMN and DAN, which is proved to have an essential role in the progression toward AD and MCI (Choo et al., 2010; Esposito et al., 2018; Sheng et al., 2019). Cortex and network importance statistics are presented in Table 3.

4. Discussions

Experiments performed in this study for ADNI and synthetic databases show that using this mapping function can substantially improve performance. Nevertheless, Further research is needed to assess the efficacy of the proposed method with other neuroimaging modalities and neurological disorders in the future.

5. Conclusions

This study proposed a method for automatically and efficiently classifying AD, EMCI, and LMCI patients using some new features that have not previously been explored. This paper made the following main contributions:

- Node2vec (Grover and Leskovec, 2016), which has been proved to be one of the successful methods for node embeddings in many fields of research (Ata et al., 2018; Peng et al., 2019; Zhao et al., 2019), has been exploited as features for Support Vector Machine and Logistic Regression classifiers in Functional Brain Networks in HCP-MMP atlas.
- A new mapping function for the construction of functional connectivity has been proposed in this study. Networks derived from this mapping function have the benefits of thresholded binary networks and weighted networks together. The proposed mapping function squeezes small correlations toward zero and expands the remaining with substantial correlations with more significant weights. The primary motivation behind the B distributed mapping function's development is that using raw correlation values as the connection strength between nodes could not be a proper solution. Since, in this study, fea-

tures are attained using a random walk procedure. In the mentioned network types, the random walker has a high probability of traversing unessential links and missing the important links. One of the crucial issues is to find a way to form a better connectivity matrix from those correlation matrices. The proposed mapping function squeezes small correlations toward zero and magnifies more significant values. In this way, the probability that the random walker moves to another nodes with a more powerful link becomes much higher.

Declaration of Competing Interest

The authors declare that they have no known competing financial interests or personal relationships that could have appeared to influence the work reported in this paper.

References

Abraham A, Pedregosa F, Eickenberg M, Gervais P, Mueller A, Kossaifi J, Gramfort A, Thirion B, Varoquaux G. Machine learning for neuroimaging with scikit-learn. Front Neuroinform 2014;8. https://doi.org/10.3389/fninf.2014.00014.

Ata SK, Ou-Yang L, Fang Y, Kwoh CK, Wu M, Li XL. Integrating node embeddings and biological annotations for genes to predict disease-gene associations. BMC Syst Biol 2018;12:138. https://doi.org/10.1186/s12918-018-0662-y.

AVANTS B, EPSTEIN C, GROSSMAN M, GEE J. Symmetric diffeomorphic image registration with cross-correlation: Evaluating automated labeling of elderly and neurodegenerative brain. Med Image Anal 2008;12(1):26–41. https://doi.org/10.1016/j.media.2007.06.004.

Behzadi Y, Restom K, Liau J, Liu TT. A component based noise correction method (CompCor) for BOLD and perfusion based fMRI. Neuroimage 2007;37(1):90–101. https://doi.org/10.1016/j.neuroimage.2007.04.042.

Bi X-a, Shu Q, Sun Qi, Xu Q, Ginsberg SD. Random support vector machine cluster analysis of resting-state fMRI in Alzheimer's disease. PLoS One 2018a;13(3): e0194479. https://doi.org/10.1371/journal.pone.0194479.

Bi XA, Xu Q, Luo X, Sun Q, Wang Z. Weighted random support vector machine clusters analysis of resting-state fMRI in mild cognitive impairment. Front Psychiatry 2018b;9:340. https://doi.org/10.3389/fpsyt.2018.00340.

Brookmeyer R, Johnson E, Ziegler-Graham K, Arrighi HM. Forecasting the global burden of Alzheimer's disease. Alzheimer's Dement 2007;3(3):186–91. https://doi.org/10.1016/j.jalz.2007.04.381.

Buckner RL, Krienen FM, Castellanos A, Diaz JC, Yeo BTT. The organization of the human cerebellum estimated by intrinsic functional connectivity. J Neurophysiol 2011;106(5):2322–45. https://doi.org/10.1152/jn.00339.2011.

Chang CC, Lin CJ. LIBSVM: A Library for support vector machines. ACM Trans Intell Syst Technol 2011;2(3):1–27. https://doi.org/10.1145/1961189.1961199.

Chen X, Zhang H, Gao Y, Wee CY, Li G, Shen D. High-order resting-state functional connectivity network for MCI classification. Hum Brain Mapp 2016;37(9):3282–96. https://doi.org/10.1002/hbm.v37.910.1002/hbm.23240.

Choo ILH, Lee DY, Oh JS, Lee JS, Lee DS, Song IC, Youn JC, Kim SG, Kim KW, Jhoo JH, Woo JI. Posterior cingulate cortex atrophy and regional cingulum disruption in mild cognitive impairment and Alzheimer's disease. Neurobiol Aging 2010;31(5):772–9. https://doi.org/10.1016/j.neurobiolaging.2008.06.015.

Cohen J. Weighted kappa: Nominal scale agreement provision for scaled disagreement or partial credit. Psychol Bull 1968;70:213–20. https://doi.org/10.1037/h0026256.

Dale AM, Fischl B, Sereno MI. Cortical surface-based analysis: I. Segmentation and surface reconstruction. Neuroimage 1999;9(2):179–94. https://doi.org/10.1006/nimg.1998.0395.

Duara R, Loewenstein DA, Shen Q, Barker W, Potter E, Varon D, Heurlin K, Vandenberghe R, Buckley C. Amyloid positron emission tomography with 18F-flutemetamol and structural magnetic resonance imaging in the classification of mild cognitive impairment and Alzheimer's disease. Alzheimer's Dement 2013;9(3):295–301. https://doi.org/10.1016/j.jalz.2012.01.006.

Dubois B, Hampel H, Feldman HH, Scheltens P, Aisen P, Andrieu S, et al. Preclinical Alzheimer's disease: definition, natural history, and diagnostic criteria. Alzheimer's Dement 2016;12(3):292–323. https://doi.org/10.1016/j.jalz.2016.02.002.

Engels MMA, Hillebrand A, van der Flier WM, Stam CJ, Scheltens P, van Straaten ECW. Slowing of Hippocampal Activity Correlates with Cognitive Decline in Early Onset Alzheimer's Disease. An MEG Study with Virtual Electrodes. Front Hum Neurosci 2016;10. https://doi.org/10.3389/fnhum.2016.00238.

Esposito R, Cieri F, Chiacchiaretta P, Cera N, Lauriola M, Di Giannantonio M, Tartaro A, Ferretti A. Modifications in resting state functional anticorrelation between default mode network and dorsal attention network: comparison among young adults, healthy elders and mild cognitive impairment patients. Brain Imaging Behav 2018;12(1):127–41. https://doi.org/10.1007/s11682-017-9686-y.

Esteban O, Markiewicz CJ, Blair RW, Moodie CA, Isik AI, Erramuzpe A, Kent JD, Goncalves M, DuPre E, Snyder M, Oya H, Ghosh SS, Wright J, Durnez J, Poldrack RA, Gorgolewski KJ. fMRIPrep: a robust preprocessing pipeline for functional MRI. Nat Methods 2019;16(1):111–6. https://doi.org/10.1038/s41592-018-0235-4.

Esteban O, Markiewicz CJ, Blair RW, Moodie CA, Isik AI, Erramuzpe A, et al. FMRIPrep: A robust preprocessing pipeline for functional MRI. BioRxiv 2018;16:111–6. https://doi.org/10.1101/306951.

Esteban O, Markiewicz CJ, Burns C, Goncalves M, Jarecka D, Ziegler E, et al. nipy/nippype: 1.5.1 2020. DOI: 10.5281/ZENODO.4035081.

Fan RE, Chang KW, Hsieh CJ, Wang XR, Lin CJ. LIBLINEAR: A library for large linear classification. J Mach Learn Res 2008;9:1871–4. https://doi.org/10.1145/1390681.1442794.

Fonov V, Evans A, McKinstry R, Almli C, Collins D. Unbiased nonlinear average age-appropriate brain templates from birth to adulthood. Neuroimage 2009;47:S102. https://doi.org/10.1016/s1053-8119(09)70884-5.

Friston KJ, Holmes AP, Worsley KJ, Poline J-P, Frith CD, Frackowiak RSJ. Statistical parametric maps in functional imaging: A general linear approach. Hum Brain Mapp 1994;2(4):189–210. https://doi.org/10.1002/hbm.v2:410.1002/hbm.460020402.

Glasser MF, Coalson TS, Robinson EC, Hacker CD, Harwell J, Yacoub E, Ugurbil K, Andersson J, Beckmann CF, Jenkinson M, Smith SM, Van Essen DC. A multi-modal parcellation of human cerebral cortex. Nature 2016;536(7615):171–8. https://doi.org/10.1038/nature18933.

Gorgolewski K, Burns CD, Madison C, Clark D, Halchenko YO, Waskom ML, et al. Nipype: A flexible, lightweight and extensible neuroimaging data processing framework in Python. Front Neuroinform 2011;5:13. https://doi.org/10.3389/fninf.2011.00013.

Greve DN, Fischl B. Accurate and robust brain image alignment using boundary-based registration. Neuroimage 2009;48(1):63–72. https://doi.org/10.1016/j.neuroimage.2009.06.060.

Grover A, Leskovec J. Node2vec: Scalable feature learning for networks. Proc. ACM SIGKDD Int. Conf. Knowl. Discov. Data Min., vol. 13-17- Augu, 2016, p. 855–64. DOI: 10.1145/2939672.2939754.

Huntenburg JM, Gorgolewski KJ, Anwander A, Margulies DS. Evaluating nonlinear coregistration of BOLD EPI and T1 images. Freie Universität Berlin; 2014.

Jack CR, Bennett DA, Blennow K, Carrillo MC, Dunn B, Haeberlein SB, et al. NIA-AA research framework: toward a biological definition of Alzheimer's disease. Alzheimer's Dement 2018;14(4):535–62. https://doi.org/10.1016/j.jalz.2018.02.018.

Jenkinson M, Bannister P, Brady M, Smith S. Improved optimization for the robust and accurate linear registration and motion correction of brain images. Neuroimage 2002;17:825–41. https://doi.org/10.1016/S1053-8119(02)91132-8.

Jie B, Liu M, Shen D. Integration of temporal and spatial properties of dynamic connectivity networks for automatic diagnosis of brain disease. Med Image Anal 2018;47:81–94. https://doi.org/10.1016/j.media.2018.03.013.

Jie B, Zhang D, Gao W, Wang Q, Wee CY, Shen D. Integration of network topological and connectivity properties for neuroimaging classification. IEEE Trans Biomed Eng 2014;61:576–89. https://doi.org/10.1109/TBME.2013.2284195.

Khazaee A, Ebrahimzadeh A, Babajani-Feremi A. Application of advanced machine learning methods on resting-state fMRI network for identification of mild cognitive impairment and Alzheimer's disease. Brain Imaging Behav 2016;10(3):799–817. https://doi.org/10.1007/s11682-015-9448-7.

Khazaee A, Ebrahimzadeh A, Babajani-Feremi A. Identifying patients with Alzheimer's disease using resting-state fMRI and graph theory. Clin Neurophysiol 2015;126(11):2132–41. https://doi.org/10.1016/j.clinph.2015.02.060.

Klein A, Ghosh SS, Bao FS, Giard J, Häme Y, Stavsky E, Lee N, Rossa B, Reuter M, Chaibub Neto E, Keshavan A, Schneidman D. Mindboggling morphometry of human brains. PLoS Comput Biol 2017;13(2):e1005350. https://doi.org/10.1371/journal.pcbi.1005350.

Lanczos C. Evaluation of Noisy Data. J Soc Ind Appl Math Ser B Numer Anal 1964;1(1):76–85. https://doi.org/10.1137/0701007.

Lehmann C, Koenig T, Jelic V, Prichep L, John RE, Wahlund L-O, Dodge Y, Dierks T. Application and comparison of classification algorithms for recognition of Alzheimer's disease in electrical brain activity (EEG). J Neurosci Methods 2007;161(2):342–50. https://doi.org/10.1016/j.jneumeth.2006.10.023.

Lindquist MA, Geuter S, Wager TD, Caffo BS. Modular preprocessing pipelines can reintroduce artifacts into fMRI data. BioRxiv 2018;40:2358–76. https://doi.org/10.1101/407676.

Makris N, Goldstein JM, Kennedy D, Hodge SM, Caviness VS, Faraone SV, Tsuang MT, Seidman LJ. Decreased volume of left and total anterior insular lobule in schizophrenia. Schizophr Res 2006;83(2-3):155–71. https://doi.org/10.1016/j.schres.2005.11.020.

Mikolov T, Sutskever I, Chen K, Corrado GS, Dean J. Distributed Representations of Words and Phrases and their Compositionality. NIPS 2013:3111–9.

Misra C, Fan Y, Davatzikos C. Baseline and longitudinal patterns of brain atrophy in MCI patients, and their use in prediction of short-term conversion to AD: Results from ADNI. Neuroimage 2009;44(4):1415–22. https://doi.org/10.1016/j.neuroimage.2008.10.031.

Muschelli J, Nebel MB, Caffo BS, Barber AD, Pekar JJ, Mostofsky SH. Reduction of motion-related artifacts in resting state fMRI using aCompCor. Neuroimage 2014;96:22–35. https://doi.org/10.1016/j.neuroimage.2014.03.028.

Paquerault S. Battle against Alzheimer's Disease. The Scope and Potential Value of Magnetic Resonance Imaging Biomarkers. Acad Radiol 2012;19(5):509–11. https://doi.org/10.1016/j.acra.2012.02.003.

Peng J, Guan J, Shang X. Predicting Parkinson's disease genes based on node2vec and autoencoder. Front Genet 2019;10. https://doi.org/10.3389/fgene.2019.00226.

Perozzi B, Al-Rfou R, DeepWalk SS. Online learning of social representations. In: Proc. ACM SIGKDD Int. Conf. Knowl. Discov. Data Min.. p. 701–10. 10.1145/2623330.2623732.

Power J, Cohen A, Nelson S, Wig G, Barnes K, Church J, Vogel A, Laumann T, Miezin F, Schlaggar B, Petersen S. Functional Network Organization of the Human Brain. Neuron 2011;72(4):665–78. https://doi.org/10.1016/j.neuron.2011.09.006.

Power JD, Mitra A, Laumann TO, Snyder AZ, Schlaggar BL, Petersen SE. Methods to detect, characterize, and remove motion artifact in resting state fMRI. Neuroimage 2014;84:320–41. https://doi.org/10.1016/j.neuroimage.2013.08.048.

Rubinov M, Sporns O. Complex network measures of brain connectivity: Uses and interpretations. Neuroimage 2010;52(3):1059–69. https://doi.org/10.1016/j.neuroimage.2009.10.003.

Satterthwaite TD, Elliott MA, Gerraty RT, Ruparel K, Loughead J, Calkins ME, Eickhoff SB, Hakonarson H, Gur RC, Gur RE, Wolf DH. An improved framework for confound regression and filtering for control of motion artifact in the preprocessing of resting-state functional connectivity data. Neuroimage 2013;64:240–56. https://doi.org/10.1016/j.neuroimage.2012.08.052.

Sharaev M., Artemov A., Kondrateva E., Ivanov S., Sushchinskaya S., Bernstein A., et al. Learning connectivity patterns via graph Kernels for fMRI-based depression diagnostics. IEEE Int. Conf. Data Min. Work. ICDMW, vol. 2018-Novem, 2019, p. 308–14. doi: 10.1109/icdmw.2018.00051.

Sheng J, Shao M, Zhang Q, Zhou R, Wang L, Xin Y. Alzheimer's disease, mild cognitive impairment, and normal aging distinguished by multi-modal parcellation and machine learning. Sci Rep 2020;10:1–10. https://doi.org/10.1038/s41598-020-62378-0.

Sheng J, Wang B, Zhang Q, Liu Q, Ma Y, Liu W, Shao M, Chen B. A novel joint HCPMMP method for automatically classifying Alzheimer's and different stage MCI patients. Behav Brain Res 2019;365:210–21. https://doi.org/10.1016/j.bbr.2019.03.004.

Son SJ, Kim J, Park H, Fan Y. Structural and functional connectional fingerprints in mild cognitive impairment and Alzheimer's disease patients. PLoS One 2017;12(3):e0173426. https://doi.org/10.1371/journal.pone.0173426.

Tang H, Guo L, Dennis E, Thompson PM, Huang H, Ajilore O, et al. Classifying Stages of Mild Cognitive Impairment via Augmented Graph Embedding. In: Lect. Notes Comput. Sci. (including Subser. Lect. Notes Artif. Intell. Lect. Notes Bioinformatics) 2019;11846. LNCS, Springer; 2019. p. 8–30. https://doi.org/10.1007/978-3-030-33226-6_4.

Tang J, Qu M, Wang M, Zhang M, Yan J, Mei Q. LINE: Large-scale information network embedding. In: Proc. 24th Int Conf. World Wide Web 2015. p. 1067–77. 10.1145/2736277.2741093.

Treiber JM, White NS, Steed TC, Bartsch H, Holland D, Farid N, et al. Characterization and correction of geometric distortions in 814 Diffusion Weighted Images. PLoS One 2016;11(3):e0152472. https://doi.org/10.1371/journal.pone.0152472.

Tustison NJ, Avants BB, Cook PA, Zheng Yuanjie, Egan Alexander, Yushkevich PA, Gee JC. N4ITK: Improved N3 bias correction. IEEE Trans Med Imaging 2010;29(6):1310–20. https://doi.org/10.1109/TMI.2010.2046908.

Tzourio-Mazoyer N, Landeau B, Papathanassiou D, Crivello F, Etard O, Delcroix N, Mazoyer B, Joliot M. Automated anatomical labeling of activations in SPM using a macroscopic anatomical parcellation of the MNI MRI single-subject brain. Neuroimage 2002;15(1):273–89. https://doi.org/10.1006/nimg.2001.0978.

de Vos F, Koini M, Schouten TM, Seiler S, van der Grond J, Lechner A, et al. A comprehensive analysis of resting state fMRI measures to classify individual patients with Alzheimer's disease. Neuroimage 2018;167:62–72. https://doi.org/10.1016/j.neuroimage.2017.11.025.

Wang S, Peterson DJ, Gatenby JC, Li W, Grabowski TJ, Madhyastha TM. Evaluation of field map and nonlinear registration methods for correction of susceptibility artifacts in diffusion MRI. Front Neuroinform 2017;11:17. https://doi.org/10.3389/fninf.2017.00017.

Wang Z, Zheng Y, Zhu DC, Bozoki AC, Li T. Classification of Alzheimer's disease, mild cognitive impairment and normal control subjects using resting-state fmri based network connectivity analysis. IEEE J Transl Eng Heal Med 2018;6:1–9. https://doi.org/10.1109/JTEHM.2018.2874887.

Xue J, Guo H, Gao Y, Wang X, Cui H, Chen Z, et al. Altered Directed Functional Connectivity of the Hippocampus in Mild Cognitive Impairment and Alzheimer's Disease: A Resting-State fMRI Study. Front Aging Neurosci 2019;11. https://doi.org/10.3389/fnagi.2019.00326.

Yeo BTT, Krienen FM, Sepulcre J, Sabuncu MR, Lashkari D, Hollinshead M, et al. The organization of the human cerebral cortex estimated by intrinsic functional connectivity. J Neurophysiol 2011;106(3):1125–65. https://doi.org/10.1152/jn.00338.2011.

Zhang T, Zhao Z, Zhang C, Zhang J, Jin Z, Li L. Classification of early and late mild cognitive impairment using functional brain network of resting-state fMRI. Front Psychiatry 2019;10:572. https://doi.org/10.3389/fpsyt.2019.00572.

Zhang X, Hu B, Ma X, Xu L. Resting-state whole-brain functional connectivity networks for MCI classification using L2-regularized logistic regression. IEEE Trans Nanobioscience 2015;14(2):237–47. https://doi.org/10.1109/TNB.2015.2403274.

Zhang Y, Brady M, Smith S. Segmentation of brain MR images through a hidden Markov random field model and the expectation-maximization algorithm. IEEE Trans Med Imaging 2001;20:45–57. https://doi.org/10.1109/42.906424.

Zhao T, Hu Y, Zang T, Cheng L. Identifying Alzheimer's disease-related proteins by LRRGD. BMC Bioinformatics 2019;20:570. https://doi.org/10.1186/s12859-019-3124-7.

Zhu C, Byrd RH, Lu P, Nocedal J. Algorithm 778: L-BFGS-B: Fortran subroutines for large-scale bound-constrained optimization. ACM Trans Math Softw 1997;23(4):550–60. https://doi.org/10.1145/279232.279236.